Image Segmentation Method Based on Fractional Varying-order Differential

Yuru Tian* and Yanshan Zhang†
* College of Computer Science and Technology, China University of Petroleum, Qingdao, China
E-mail: tyr0228@foxmail.com
† School of Intelligent Engineering, Zhengzhou University of Aeronautics, Zhengzhou, China
E-mail: yanshan@zua.edu.cn

***Abstract*—Image segmentation plays a very important role in many applications. At present, the most difficult problem of image segmentation is segmenting intensity inhomogeneous images, some hybrid methods have better segmentation results than the traditional methods. In this paper, a new hybrid level set method based on fractional-varying-order differential curvature is proposed. We define a new curve evolution curvature calculated by fractional-varying-order differential according to the gradient of the level set function, so that the diverse order differential can be used in a whole curve evolution at the same time, which can describe the image edge more accurately. The energy functional for the proposed model consists of three terms: local term, length term and penalty term. The evolution of the level set function is the gradient flow that minimizes the overall energy functional. Experimental results for both synthetic and real images show desirable performance of our method. The Dice similarity coefficient are employed as the comparative quantitative measures for the segmented results.**

I. Introduction

The existing image segmentation methods can be classified into four categories: the clustering-based methods[1], [2], the graph-cut-based methods[3], [4], neural-network-based methods[5], [6] and active-based methods[7], [8]. The clustering-based methods assume each pixel as a sample and pixels belonging to the same class are subject to a specific distribution, then the image is segmented by clustering methods like K-means and fuzzy C-means. The clustering methods have high efficiency while they are sensitive to initial clustering centers. Besides, the clustering number needs to be set manually. The graph-cut-based methods take the correlations between pixels into consideration and transform the segmentation problem into a graph partition problem, then a cut energy model is built and the cut which minimizes the energy is chosen to be the segmentation curve. The main shortage of the graph-cut-based methods is that it is difficult to construct accurate weights for the correlations between pixels, which often leads to under-segmentation or over-segmentation in complicated regions. Recently, neural-network-based methods have been developed to perform a variety of tasks including the semantic segmentation, and shows a vast range of prospects. However, it needs lots of images to train the network and the output often gives a rough but not fine segmentation in tiny area, while fine details are crucial in medical image analysis. Another branch of methods are based on the active contour model. Since the active contour model can give closed boundaries and performs stably, it has been used to develop new algorithms. Until now the active-contour-based models are still effective and prevalent. Generally speaking, the existing active contour methods can be classified into two types: edge-based models and region-based models. Each of them has its own advantage and disadvantage. Edge-based model uses image gradient information to guide curve evolution. The method detects the boundary of different regions, which can locate the edge accurately, but weak edge can not be detected and it depends on location of initial curve. So the detected edge can not be closed and it is sensitive to noise. One of them is the famous geodesic active contour model[9] , which is derived from the snake model[10] and defines a gradient-based edge detector function. Because of the local limitation, this models are sensitive to noise and have difficulty in detecting weak boundary. Region based active contour model does not utilize image gradient, but uses local information of image to evolve curve, which can better detect weak edges. The initial contour can start anywhere in the image, and the interior contours can be automatically detected. One of the most popular region-based models is the CV model[11], which has been successfully used in binary phase segmentation with the assumption that each image region is statistically homogeneous. However, the CV model does not work well for the images with intensity inhomogeneity, because it assumes that each region is statistically homogeneous and the intensities within the area of foreground and background always maintain constant, respectively. To overcome this defect, many methods have been proposed to overcome the difficulty of segmenting intensity inhomogeneity images. For example, Vese and Chan [12] and Tsai et al.[13] proposed piece-wise smooth (PS) models by minimizing the MS functional[14], which replaced the piece-wise constant intensity by piece-wise smooth intensity. Although these PS models have certain capability of handling the intensity inhomogeneity, they are computationally expensive and the gain in segmentation accuracy is limited. Then Li et al.[15] proposed a LBF model by incorporating a kernel function to define local binary fitting energy in a variational formulation. Zhang et al.[16] exploited local image region statistics to present a level set method for segmenting images with intensity inhomogeneity. Liu and Peng [17] proposed a local region-based CV model by considering the image local characteristics. Wang et al.[18] proposed an alternative LCV

model by utilizing the difference image information.

The fractional-order PDE is an important branch of the PDEs. The main advantage of this method is to handle the topological changes automatically which is generally impossible for the traditional parametric active contour model. Cuesta[19] proposed fractional-order linear integral-differential equations, which interpolated heat equations and wave equations using the Riemann-Liouville fractional derivative. Mathieu et al.[20] used fractional derivative to detect the image edges. Ren [21] present a new adaptive active contour model based on fractional order differentiation. Chen et al.[22] proposed an adaptive-weighting active contour model, which incorporates image gradient, local environment and global information into a framework. On the basis of fractional differential, we proposed fractional-varying-order differential by matrix operation, the differential orders of different parts of the image can be variable. Thus, we can gain more detailed image information so that we can process it conveniently.

In summary, we present a new active contour model based on fractional-varying-order differential. The energy functional for the proposed model consists of three terms: local term, length term and penalty term. We use a new curve evolution curvature calculated by the fractional-varying-order differential to form a novel length term and penalty term. By incorporating the local term, the length term and penalty term this model can describe the original image more accurately, and be robustness to noise. In order to ensure stable evolution of the level set function, a penalty term[23] is added into the proposed model. The evolution of the level set function is the gradient flow that minimizes the overall energy functional. Experimental results for both synthetic and real images show desirable performance of our method.

The remainder of this paper is organized as follows. In Section 2, we present a brief introduction of several related works. We describe the proposed active contour model in details in Section 3. Section 4 presents the experimental results and comparisons on real and synthetic images. Finally, conclusions are drawn in Section 5.

II. The related models and background

A. CV Model

By simplifying the Mumford-Shah model[14], Chan and Vese [11] proposed a region-based active contour model. This model is to utilize regional mean gray values to decide the contour and divide the image into the targets and background. Let Ω be the image domain, and $I(x,y) : \Omega \rightarrow R$ is a given image function, where x, y represent horizontal and vertical coordinates of pixels respectively, and $I(x,y)$ denotes the intensity at a point (x,y). This model is formulated by minimizing the following energy functional:

$$\begin{aligned} E^{CV}(C,c_1,c_2) &= \lambda_1 \int_{inside(C)} |I(x,y)-c_1|^2 \\ & H(\phi(y))dxdy + \lambda_2 \int_{outside(C)} \\ & |I(x,y)-c_2|^2(1-H(\phi(y)))dxdy \end{aligned} \quad (1)$$

where λ_1, λ_1 are fixable parameters, inside(C) and outside(C) represent the region inside and outside of the contour C, c_1 and c_2 are the mean gray value of the inside or outside region respectively. $H(\varphi)$ is the Heaviside function. Notation $\delta(\cdot)$ indicates the Dirac function and it is defined as the derivative of the Heaviside function $H(\cdot)$:

$$H(z) = \begin{cases} 1, & z \geq 0 \\ 2, & z < 0 \end{cases}, \quad (2)$$

$$\delta(z) = \frac{d}{dz}H(z) = \begin{cases} 0, & z \neq 0 \\ +\infty, & z = 0 \end{cases} \quad (3)$$

By minimizing (1), we can obtain C_1 and C_2:

$$\begin{cases} C_1 = \frac{\int_\Omega I(x,y)H(\phi(x,y))dxdy}{\int_\Omega H(\phi(x,y))dxdy} \\ C_2 = \frac{\int_\Omega I(x,y)(1-H(\phi(x,y)))dxdy}{\int_\Omega (1-H(\phi(x,y)))dxdy} \end{cases} \quad (4)$$

By introducing a length term $\int_\Omega \delta(\phi(x,y))|\nabla\phi(x,y)|$dxdy (where ∇ represents the gradient operator) and an area term $\int_\Omega H(\phi(x,y))dxdy$, which are used to regularize the contour. Then minimizing these terms together, we can obtain the following variational formulation:

$$\frac{\partial\varphi}{\partial t} = \delta(\phi)[\mu div(\frac{\nabla\phi}{|\nabla\phi|}) - \nu - \lambda_1(I-c_1)^2 + \lambda_2(I-c_2)^2] \quad (5)$$

where parameters $\mu \geq 0$,$\nu \geq 0$. μ is a scaling parameter, it controls the smoothness of zero level set. If it is small enough, small objects are likely to be extracted, if it is large enough, big objects are likely to be detected. And ν increases the propagation speed.

In order to compute the partial differential equation in (5), discontinuous functions $H(\varphi)$ and $\delta(\varphi)$ need to be approximated by regularized version $H_\varepsilon(\varphi)$, $\delta_\varepsilon(\varphi)$. In general, the regularized Heaviside function and Dirac function are selected as follows:

$$H_\varepsilon(Z) = \frac{1}{2}(1 + \frac{2}{\pi}\arctan(\frac{z}{\varepsilon})) \quad (6)$$

$$\delta_z = \frac{1}{\pi}\frac{\varepsilon}{\varepsilon^2 + z^2}, z \in R \quad (7)$$

where R represents the set of real number and ε is a small value in the denominator to avoid the singularities. ε is also a predefined parameter for control the speed of the function $H_\varepsilon(z)$ rising from 0 to 1. CV model has good performance in detection of objects whose boundaries are not necessarily defined by gradient or with weak boundaries. However, it generally fails to segment images with intensity inhomogeneity.

B. LBF MODEL

The local statistical information of the LBF model[15] is obtained by introducing a kernel function. Consider a given vector valued image $I : \Omega \rightarrow \Re^d$, where $\Omega \subset \Re^d$ is the image domain, and d $\geq$ 1 is the dimension of the vector $I(\boldsymbol{x})$. For gray level images, d=1, for color images, d=3. Let C be

a contour in the image domain Ω, They defined the energy functional as follows

$$\begin{aligned} E^{LBF}(\phi, f_1, f_2) &= \lambda_1 \int_\Omega [\int_\Omega K_\sigma(\boldsymbol{x}-\boldsymbol{y})|I(\boldsymbol{y})-f_1(\boldsymbol{x})|^2 \\ &\quad H(\phi(\boldsymbol{y}))d\boldsymbol{y}]d\boldsymbol{x} \\ &\quad +\lambda_2 \int_\Omega [\int_\Omega K_\sigma(\boldsymbol{x}-\boldsymbol{y})|I(\boldsymbol{y})-f_2(\boldsymbol{x})|^2 \\ &\quad (1-H(\phi(\boldsymbol{y})))d\boldsymbol{y}]d\boldsymbol{x} \end{aligned} \tag{8}$$

where K_σ is the Gaussian kernel function with standard deviation σ, $\lambda_1 > 0$, $\lambda_2 > 0$, are fixed parameters. Keeping level set function ϕ fixed and minimizing the energy functional (8) with regard to local center f_1 and f_2, we can obtain the following equation

$$f_1(\boldsymbol{y}) = \frac{K_\sigma(\boldsymbol{x}) * [H_\varepsilon(\phi(\boldsymbol{x}))I(\boldsymbol{x})]}{K_\sigma(\boldsymbol{x}) * [H_\varepsilon(\phi(\boldsymbol{x}))]} \tag{9}$$

$$f_2(\boldsymbol{y}) = \frac{K_\sigma(\boldsymbol{x}) * [(1-H_\varepsilon(\phi(\boldsymbol{x})))I(\boldsymbol{x})]}{K_\sigma(\boldsymbol{x}) * [1-H_\varepsilon(\phi(\boldsymbol{x}))]} \tag{10}$$

Although the LBF model can effectively segment inhomogeneous images, it is sensitive to initial contour.

C. LIC MODEL

This model is proposed by Li et al.[24] based on bias field estimation and local intensity clustering property.

1) Bias field estimation : For the real-world images, an observed image I can be modeled as

$$I = bJ + n \tag{11}$$

where J is the true image which is an intrinsic physical property of the objects being imaged, thus it can be approximately assumed to be piecewise constant; b is the intensity inhomogeneity component which is referred to as a bias field(or shading image), and n is additive noise which can be assumed to be zero-mean Gaussian noise.

Based on the above properties, Li et al. proposed two assumptions: (1) The bias field b is slowly varying, which implies that b can be well approximated by a constant in a neighborhood of each point in the image domain. (2) The true image J approximately takes N distinct constant values , c_1..., c_N in disjoint regions, $\Omega_1, \cdots, \Omega_N$, respectively, where ${\Omega_i}_{i=1}^N$ forms a partition of the image domain, i.e. $\Omega = \cup_{i=1}^N \Omega_i$ and $\Omega_i \cap \Omega_j = \phi$ for $i \neq j$.

2) Local intensity clustering property: Based on the image model in (12) and the assumptions (1) and (2), Li et al.used a property of local intensities, which is referred to as a local intensity clustering property as described and justified below. They considered a circular neighborhood with a radius ρ centered at each point $\boldsymbol{y} \in \Omega$, defined by $\vartheta_{\boldsymbol{y}} =: \{\boldsymbol{x} : |\boldsymbol{x}-\boldsymbol{y}| \leq \rho\}$. The partition ${\Omega_i}_{i=1}^N$ of the entire domain Ω induces a partition of $\vartheta_{\boldsymbol{y}}$. For a slowly varying bias field b, the values $b(\boldsymbol{x})$ for all $\boldsymbol{x}$ in the circular neighborhood $\vartheta_{\boldsymbol{y}}$ are close to $b(\boldsymbol{y})$, i.e.

$$b(\boldsymbol{x}) \approx b(\boldsymbol{y}), \ for \ \boldsymbol{x} \in \vartheta_{\boldsymbol{y}} \tag{12}$$

Thus, the intensities $b(\boldsymbol{x})J(\boldsymbol{x})$ in each subregion $\vartheta_{\boldsymbol{y}} \cap \Omega_i$ are close to the constant $b(\boldsymbol{y})$, i.e.

$$b(\boldsymbol{x})J(\boldsymbol{x}) \approx b(\boldsymbol{y})c_i, \ for \ \boldsymbol{x} \in \vartheta_{\boldsymbol{y}} \cap \Omega_i \tag{13}$$

Then, in view of the image model in (12), we have

$$I(\boldsymbol{x}) \approx b(\boldsymbol{y})c_i \approx b(\boldsymbol{y})c_i + n(\boldsymbol{x}) \ for \ \boldsymbol{x} \in \vartheta_{\boldsymbol{y}} \cap \Omega_i \tag{14}$$

where $n(\boldsymbol{x})$ is additive zero-mean Gaussian noise. Therefore, the intensities in the set $I_{\boldsymbol{y}}^i = I(\boldsymbol{x}) : \boldsymbol{x} \in \vartheta_{\boldsymbol{y}} \cap \Omega_i$ form a cluster with cluster center, which can be considered as samples drawn from a Gaussian distribution with mean m_i. Obviously, the clusters $I_{\boldsymbol{y}}^1, \cdots, I_{\boldsymbol{y}}^N$, are well-separated, with distinct cluster centers $m_i \approx b(\boldsymbol{y})c_i, i = 1, ..., N$, because the constants are distinct and the variance of the Gaussian noise n is assumed to be relatively small. This local intensity clustering property is used to formulate the proposed method for image segmentation and bias field estimation as follows.

3) Energy Formulation: Li et al. applied the standard K-means clustering to classify these intensities according to the above described local intensity clustering property indicates that the intensities in the neighborhood can be classify into N clusters,with center $m_i \approx b(\boldsymbol{y})c_i, i = 1, ..., N$

Then the two-phase energy functional as follows

$$F(\phi, c, b) = \varepsilon(\phi, c, b) + \nu(\phi) + \mu(\phi) \tag{15}$$

The $\varepsilon(\phi, c, b)$ is defined by

$$\varepsilon = \int \left(\sum_{i=1}^N \int K(\boldsymbol{y}-\boldsymbol{x})(|I(\boldsymbol{x}) - b(\boldsymbol{y})c_i|)^2 M_i(\phi(\boldsymbol{x}))d\boldsymbol{x} \right) d\boldsymbol{y} \tag{16}$$

where the membership functions defined by

$$\begin{cases} M_1(\phi) = H(\phi) \\ M_2(\phi) = 1 - H(\phi) \end{cases} \tag{17}$$

The energy term $L(\phi)$ is defined by

$$L(\phi) = \int |\nabla H(\phi)|d\boldsymbol{x} \tag{18}$$

The energy term $R_p(\phi)$ is defined by

$$R_p(\phi) = \int p(|\nabla\phi|)d\boldsymbol{x} \tag{19}$$

where $p(s) = (1/2)(s-2)^2$

With respect to c, we can obtain the follow equation

$$\hat{c}_i = \frac{\int (b * K)Iu_i d\boldsymbol{y}}{\int (b^2 * K)u_i d\boldsymbol{y}}, \ i = 1, ..., N \tag{20}$$

with $u_i(\boldsymbol{y}) = M_i(\phi(\boldsymbol{y}))$

Equally, with respect to b, we can obtain the follow equation

$$\hat{b} = \frac{(IJ^1) * K}{J^2 * K} \tag{21}$$

where $J^1 = \sum_{i=1}^N c_i u_i$ and $J^2 = \sum_{i=1}^N c_i^2 u_i$

This model can segment images with intensity inhomogeneities and more robust to contour initialization. Moreover, this model is much more efficient than the LBF model.

D. The fractional order differential

The definition of fractional order differential is not unified until now. The usual definitions among them include: Grnwald-Letnikov derivative, Riemman-Liouville fractional derivative, Caputo fractional derivative, Laplace-domain fractional derivative, frequency-domain (Fourier domain) fractional derivative. For example, the famous Riemman-Liouville fractional derivative can be defined as follows:

Let $f(t)$ be a continuous function and $f(t) : (0, +\infty) \longrightarrow R$, then define the $\alpha(\alpha > 0)$-order Riemman-Liouville fractional derivative as:

$$D_\alpha f(t) = \frac{1}{\Gamma(n-\alpha)} \left(\frac{d}{dt}\right)^n \int_0^t \frac{f(s)}{(t-s)^{\alpha-n+1}} ds \tag{22}$$

where $n = [\alpha] + 1$ and $[\alpha]$ denotes the integer part of α.

Other ways of definition is the frequency-domain fractional order differential. For a given function of a single variable $f(t)$, it Fourier transform is defined as follow:

$$F(\omega) = \int_R f(t) e^{-j\omega t} dt \tag{23}$$

According to the differential property of Fourier transform, the equivalent formulation of the n-order derivative in the Fourier domain is:

$$D^n f = f^n(t) \leftrightarrow F(f^n(t)) = (j\omega)^n F(\omega) \tag{24}$$

where n is a non-negative integer, "$\leftrightarrow$" represents the Fourier transform pair. It can be shown straightforwardly that the Fourier domain expression of the α-order differential:

$$F(D^\alpha f(t)) = (j\omega)^\alpha F(\omega) \tag{25}$$

where α the can be any positive real number. Thus, the fractional order differential expression of the function $f(t)$ in frequency domain is defined as:

$$D^\alpha f(t) = F^{-1}((j\omega)^\alpha F(\omega)), \alpha \in \Re^+ \tag{26}$$

where $\Re^+$ is the set of positive real number, and F^{-1} is the inverse Fourier transform operator. Thus the fractional order partial differential of the two-dimensional function $g(x, y)$ can be defined as follows:

$$\begin{cases} D_x^\alpha g(x,y) = F^{-1}(j\omega_1)^\alpha G(\omega_1, \omega_2) \\ D_y^\alpha g(x,y) = F^{-1}(j\omega_2)^\alpha G(\omega_1, \omega_2) \end{cases} \tag{27}$$

According to the translation property of the two-dimension DFT, the center difference schemes of the any order derivative in the Fourier domain can be defined as:

$$\begin{cases} D_x^\alpha g(x,y) = F^{-1}[(1 - \exp(-2\pi j\omega_1/m))^\alpha \\ \quad \exp(\pi j\alpha\omega_1/m) G(\omega_1, \omega_2)] \\ D_y^\alpha g(x,y) = F^{-1}[(1 - \exp(-2\pi j\omega_2/m))^\alpha \\ \quad \exp(\pi j\alpha\omega_2/m) G(\omega_1, \omega_2)] \end{cases} \tag{28}$$

The fractional order differential has the characteristics of increasing the low frequency component of the signal while preserving the high frequency component of the signal nonlinearly. Therefore, fractional order differential has gained more and more attention and application in the field of image processing. In this paper we use the frequency-domain fractional differential, because it is easy to compute numerically owing to the fast discrete Fourier transform.

III. The proposed model

A. Fractional-Varying-Order Differential

First, we calculate the gradient information of the image, because the edge of the image exists in the gradient information. Then we suppose$A = (a_{ij})_{n\times m}$is a $n \times m$ matrix, and its value is obtained by the following operation after obtaining the image gradient information.

$$A = 2 \times (|\nabla u_n| + 1) \div (|\nabla u_n| + 0.8) \tag{29}$$

In other words, we get the order of the fractional derivative by the gradient of the image. The range of gray value of the image is [0,255], the range of gradient can be obtained by difference is [0,255], then the range of A is [2,2.5], and then the fractional order differential operation is carried out according to the order matrix. The fractional vary-order differential operator with different orders of each pixel point is obtained by:

$$D_{\mathbf{A}} := \begin{pmatrix} D_{a_{11}} & D_{a_{12}} & \cdots & D_{a_{1m}} \\ D_{a_{21}} & D_{a_{22}} & \cdots & D_{a_{2m}} \\ \vdots & \vdots & \ddots & \vdots \\ D_{a_{n1}} & D_{a_{n2}} & \cdots & D_{a_{nm}} \end{pmatrix}, \tag{30}$$

Thus, we define the fractional-varying-order derivative in the frequency domain as

$$D_{\vec{a}} f(t) \leftrightarrow (j\vec{\omega})^{\vec{a}} \hat{f}(\vec{\omega}) \tag{31}$$

where $\vec{a}$ is an appropriate vector. It is obvious that the semi-group property of fractional-varying-order derivative operators holds, namely

$$(D_{\vec{a}})(D_{\vec{b}})f = (D_{\vec{b}})(D_{\vec{a}})f = (D_{\vec{a}+\vec{b}})f \tag{32}$$

where vectors $\vec{\alpha}$,$\vec{\beta}$ have the same dimension.

For any $g(x, y) \in L^2(R^2)$, the corresponding two dimensional$(2-D)$ Fourier transform is

$$\hat{g}(\omega_1, \omega_2) = \int_R g(x,y) exp[-j(\omega_1 x + \omega_2 y)] dxdy \tag{33}$$

Thus, the corresponding fractional-varying-order partial derivatives are

$$\begin{cases} D_{Ax} g = F^{-1}[(j\omega_1)^A \hat{g}(\omega_1, \omega_2)] \\ D_{Ay} g = F^{-1}[(j\omega_2)^A \hat{g}(\omega_1, \omega_2)] \end{cases} \tag{34}$$

where A is a $n \times m$ matrix, F^{-1} is an inverse $2-D$ Fourier transform operator. So the corresponding A-order differential and divergence of image u can be updated to

$$D_A u(x,y) = (D_{Ax} u, D_{Ay} u) \tag{35}$$

B. Energy Formulation

Based on LIC model and fractional varying-order differential, we put up forward our new energy functional model. Our proposed model also consist three parts: the local term E^L, the length(or regulation) term E^R, and the penalty term E^P. We adapt the first term of LIC model as our local term E^L in our energy functional because of their good performance in various applications. In order to get more details to get a more detailed segmentation effect, we use D_A in place of tradition differential to get new the length term and the penalty term. The new energy term E^R and E^P are defined by

$$E^R(\phi) = \int |H(D_A\phi)|d\boldsymbol{x} \tag{36}$$

$$E^L(\phi) = \int p|D_A\phi|d\boldsymbol{x} \tag{37}$$

The final energy functional can be described as

$$\begin{aligned} E &= \int (\sum_{i=1}^{N} \int K(\boldsymbol{y}-\boldsymbol{x})(|u(\boldsymbol{x})-b(\boldsymbol{y})c_i|)^2 \\ &\quad M_i(\phi(\boldsymbol{x})d\boldsymbol{x})d\boldsymbol{y} \\ &\quad + \int |D_A H(\phi)|d\boldsymbol{x} + \int p(D_A|\phi|)d\boldsymbol{x} \end{aligned} \tag{38}$$

By exchanging the order of integrations, we have

$$\begin{aligned} E &= \int \sum_{i=1}^{N} \left(\int K(\boldsymbol{y}-\boldsymbol{x})(|u(\boldsymbol{x})-b(\boldsymbol{y})c_i|)^2 d\boldsymbol{y} \right) \\ &\quad M_i(\phi(\boldsymbol{x})d\boldsymbol{x}) \\ &\quad + \nu \int |D_A H(\nabla\phi)|d\boldsymbol{x} + \mu \int p(D_A|\nabla\phi|)d\boldsymbol{x} \end{aligned} \tag{39}$$

The Euler-Lagrange equation of the energy functional is solved by using the variational method:

$$\frac{\partial F}{\partial \phi} - \frac{d}{d\boldsymbol{x}}\left(\frac{\partial F}{\partial \phi_{\boldsymbol{x}}}\right) - \frac{d}{d\boldsymbol{y}}\left(\frac{\partial F}{\partial \phi_{\boldsymbol{y}}}\right) = 0 \tag{40}$$

Among them,

$$\frac{\partial F}{\partial \phi} = \delta(\phi)(e_1 - e_2) \tag{41}$$

$$\begin{cases} \frac{\partial F}{\partial \phi_{\boldsymbol{x}}} = \nu\delta(\phi)\frac{\phi_{\boldsymbol{x}}}{|\nabla\phi|} + \mu\left(\frac{|\nabla\phi|-1}{|\nabla\phi|}\cdot\phi_{\boldsymbol{x}}\right) \\ \frac{\partial F}{\partial \phi_{\boldsymbol{y}}} = \nu\delta(\phi)\frac{\phi_{\boldsymbol{y}}}{|\nabla\phi|} + \mu\left(\frac{|\nabla\phi|-1}{|\nabla\phi|}\cdot\phi_{\boldsymbol{y}}\right) \end{cases} \tag{42}$$

$$\begin{cases} \frac{d}{dx}\left(\frac{\partial F}{\partial \phi_{\boldsymbol{x}}}\right) = \nu\delta(\phi)\frac{d}{dx}\left(\frac{\phi_{\boldsymbol{x}}}{|\nabla\phi|}\right) + \mu\frac{d}{dx}\left(\frac{|\nabla\phi|-1}{|\nabla\phi|}\cdot\phi_{\boldsymbol{x}}\right) \\ \frac{d}{dy}\left(\frac{\partial F}{\partial \phi_{\boldsymbol{y}}}\right) = \nu\delta(\phi)\frac{d}{dy}\left(\frac{\phi_{\boldsymbol{y}}}{|\nabla\phi|}\right) + \mu\frac{d}{dy}\left(\frac{|\nabla\phi|-1}{|\nabla\phi|}\cdot\phi_{\boldsymbol{y}}\right) \end{cases} \tag{43}$$

The minimization of the energy in (39) with respect to the variable can be performed by solving the following gradient flow equations:

$$\begin{aligned} \frac{\partial\phi}{\partial t} &= -\frac{\partial F}{\partial\phi} + \frac{d}{d\boldsymbol{x}}\left(\frac{\partial F}{\phi_{\boldsymbol{x}}}\right) + \frac{d}{d\boldsymbol{y}}\left(\frac{\partial F}{\phi_{\boldsymbol{y}}}\right) \\ &= -\delta(\phi)(e_1-e_2) + \nu\delta(\phi)div(\frac{\nabla\phi}{|\nabla\phi|}) \\ &\quad +\mu[div(\nabla\phi) - div(\frac{\nabla\phi}{|\nabla\phi|})] \\ &= -\delta(\phi)(e_1-e_2) + \nu\delta(\phi)K \\ &\quad +\mu[div(\nabla\phi) - K] \end{aligned} \tag{44}$$

where

$$e_i = \int K(\boldsymbol{y}-\boldsymbol{x})(|u(\boldsymbol{x})-b(\boldsymbol{y})c_i|)^2 d\boldsymbol{y} \ (i=1,2) \tag{45}$$

Here K is the curvature of the contour, and we calculate it by

$$K = D_{A\boldsymbol{x}}\phi + D_{A\boldsymbol{y}}\phi \tag{46}$$

C. Implementation And Algorithm

The implementation and algorithm of this model consists of the following steps:
1.Initialize the level set function ϕ to a function ϕ_0. Then, construct the initial contour C.
2.Calculate the contour curvature K by (46).
3.Update $\phi_{i,j}^{k+1} = \phi_{i,j}^{k} + \Delta t \cdot A(u_{i,j}^{k})$, where is the approximation of the right hand side in (44).
4.Updata $\hat{i}$, $\hat{b}$ by (20), (21).
5.Check if the set number of iterations is reached. If not, return to step 2.

IV. Experimental results

In this section, we show experimental results from segmentation of various synthetic and real images, with different types of contours and shapes. We also compare results of the proposed model with the CV model, the LBF model and the LIC model. In addition, we use Dice similarity coefficient which defined by :

$$DSC = \frac{2N(S_1 \bigcap S_2)}{N(S_1) + N(S_2)} \tag{47}$$

where N is the number of pixels in the enclosed region. The closer the DSC value is to 1, the better segmentation is. All the experiments are carried out by Matlab(R2017b) in the Lenovo DESKTOP-G20HT3F with Intel(R) Core(TM) i7-7700 CPU @ 3.60GHz processer. The paramenters are set as follows: $\mu = 1.0$, $\nu = 0.001 \times 255^2$, $\Delta t = 0.1$and ρ should be relatively smaller for images with more localized intensity inhomogeneities.

Firstly, we applied our method to a synthetic image in Fig. 1 with four different initializations of the contour and the corresponding results. In this four different initializations, we can see that these different initial contours can finally capture the boundary of the objects from these figures. It confirms that our model not be effected by different initial contours.

Next, in order to prove that our segmentation result is more robust, we used our model to segment the image under

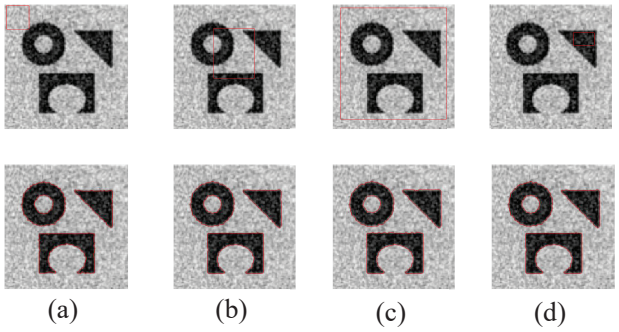

Fig. 1. Segmentation results of our model with different intializations. Top row: original images with different initializations. Bottom row: corresponding segmentation results.

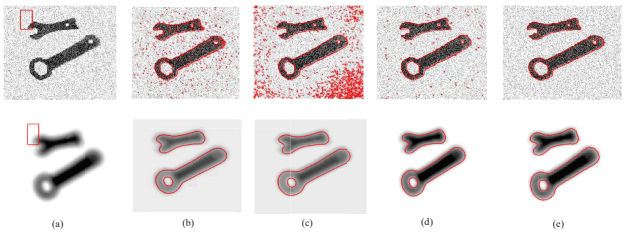

Fig. 2. Segmentation results of our model with noise and blur. Top row is the original images with noise. Bottom row is the original images with blur.(a) Original images; (b) segmentation results of CV model; (c) segmentation results of LBF model; (d) segmentation results of LIC model and (e) segmentation results of our model.

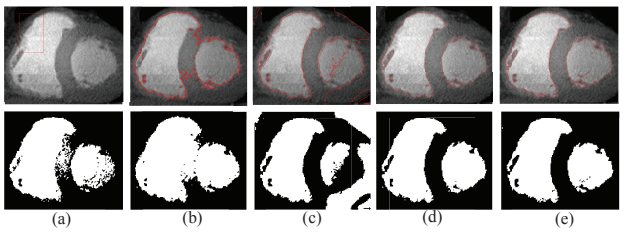

Fig. 3. Performance of our method and the CV model, the LBF model, the LIC model in different MR image. The first row:(a) Original images; (b) segmentation results of CV model; (c)segmentation results of LBF model; (d) segmentation results of LIC model and (e)segmentation results of our model. The second row:(a) ground truth; (b) white matter segmentation of CV model; (c)white matter segmentation of LBF model; (d) white matter segmentation of LIC model and (e)white matter segmentation of our model.

the conditions of noise and blur on Fig. 2. The results are compared with those of other models. From the first row images, we can see our model can still get better segmentation results in the presence of noise compared with other models. Under the condition of blurring, because the edges of the image become less clear, the contours of other models are slightly reduced in. Compared with other models, our model can resist this change and without obvious contour distortion.

Lastly, we compare our model with the CV model, the LBF model and the LIC model on Fig. 3 and Fig. 6. As shown in these results we can see that the CV model

TABLE I
THE NUMBER OF ITERATIONSDSCCPU TIME AND AVERAGE CPU TIME OF THE CV MODEL, THE LBF MODEL, THE LIC MODEL AND OUR MODELS OF FIG.3 IMAGES.

models	Iterations	DSC	CPU time	Average CPU time
CV	1000	0.9314	14.8045	0.0148
LBF	50	0.7190	13.1041	0. 2621
LIC	20	0.9143	4.8828	0.2441
OUR	20	0.9297	9.2977	0.4649

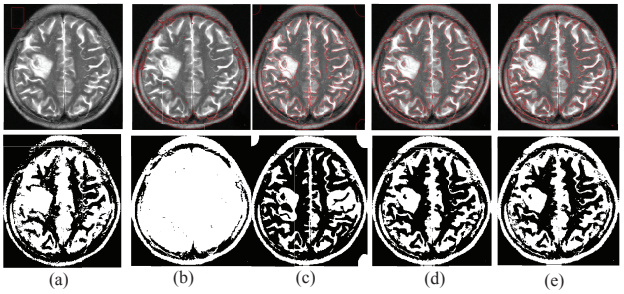

Fig. 4. Performance of our method and the CV model, the LBF model, the LIC model in different MR image. The first row:(a) Original images; (b) segmentation results of CV model; (c)segmentation results of LBF model; (d) segmentation results of LIC model and (e)segmentation results of our model. The second row:(a) ground truth; (b) white matter segmentation of CV model; (c)white matter segmentation of LBF model; (d) white matter segmentation of LIC model and (e)white matter segmentation of our model.

TABLE II
THE NUMBER OF ITERATIONSDSCCPU TIME AND AVERAGE CPU TIME OF THE CV MODEL, THE LBF MODEL, THE LIC MODEL AND OUR MODELS OF FIG.4 IMAGES.

models	Iterations	DSC	CPU time	Average CPU time
CV	1000	0.7515	55.4584	0.0555
LBF	50	0.7568	123.4280	2.4686
LIC	20	0.8448	5.1012	0.2551
OUR	20	0.8540	6.8016	0.3401

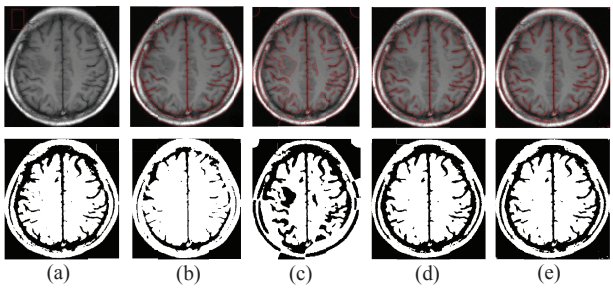

Fig. 5. Performance of our method and the CV model, the LBF model, the LIC model in different MR image. The first row:(a) Original images; (b) segmentation results of CV model; (c)segmentation results of LBF model; (d) segmentation results of LIC model and (e)segmentation results of our model. The second row:(a) ground truth; (b) white matter segmentation of CV model; (c)white matter segmentation of LBF model; (d) white matter segmentation of LIC model and (e)white matter segmentation of our model.

cannot segment preferably intensity inhomogeneity from these

TABLE III
THE NUMBER OF ITERATIONSDSCCPU TIME AND AVERAGE CPU TIME OF THE CV MODEL, THE LBF MODEL, THE LIC MODEL AND OUR MODELS OF FIG.5 IMAGES.

models	Iterations	DSC	CPU time	Average CPU time
CV	1000	0.9262	56.0668	0.0561
LBF	50	0.0.7641	120.3080	2.4062
LIC	20	0.9617	4.9140	0.2457
OUR	20	0.9657	7.1136	0.3557

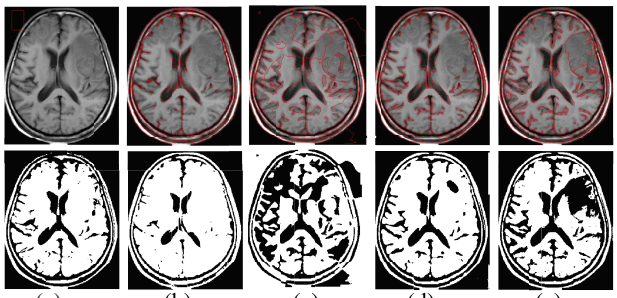

Fig. 6. Performance of our method and the CV model, the LBF model, the LIC model in different MR image. The first row:(a) Original images; (b) segmentation results of CV model; (c)segmentation results of LBF model; (d) segmentation results of LIC model and (e)segmentation results of our model. The second row:(a) ground truth; (b) white matter segmentation of CV model; (c)white matter segmentation of LBF model; (d) white matter segmentation of LIC model and (e)white matter segmentation of our model.

TABLE IV
THE NUMBER OF ITERATIONSDSCCPU TIME AND AVERAGE CPU TIME OF THE CV MODEL, THE LBF MODEL, THE LIC MODEL AND OUR MODELS OF FIG.6 IMAGES.

models	Iterations	DSC	CPU time	Average CPU time
CV	1000	0.7987	65.2708	0.0653
LBF	50	0.5201	38.6414	0. 7728
LIC	5	0.8523	15.9277	3.1855
OUR	5	0.8845	38.2982	7.6596

images and because the LBF model is affected by level set initialization, so it does not perform well in the initial contour we set. Compared with LIC model, in the image with large difference in gray value(see Fig. 3-Fig. 5), the segmentation regions obtained by these two methods are relatively close, but our method will have more fluctuation in the segmentation edge part. The edges of this resulting conforms to the actual situation, reflected in the DSC value is the value slightly bigger than the LIC models. In images with close gray values(see Fig. 6), it is obvious that our model will distinguish more regions than the LIC model. This is because we used diverse differential orders to the different parts of the curve and gained more detailed information so we can see that edge is more refined than the LIC model and it can handle some details better. As shown in the DSC values of each table, the segmentation accuracy is quantitatively verified by evaluating these results. These experiments demonstrate the robustness and accuracy of our model. And we can see that in average CPU time, CV model is the fastest image segmentation method, because the c_1c_2 in its energy functional is constant and there is no complex calculation. But it cannot accurately represent the intensity of the image inside and outside the contour, so it cannot segment the image with intensity inhomogeneity. The speed of image segmentation by LBF model is related to the size of the image. The larger the image, the longer the time it takes, and conversely the shorter it is. In the image with large difference in gray value(see Table. I -Table. III), we can see that there is little difference in average CPU time between the LIC model and our model, but our model is slightly higher than the LIC model. And in images with close gray values(see Table. IV), our model is more higher than LIC model. This is because our model uses fractional differentiation in the image gradient part, which takes a long time to calculate, but we get a more accurate segmentation than LIC model.

V. CONCLUSION

In this paper, we proposed a new image segmentation model based LIC model and apply fractional-varying-order differential to this model. Application of fractional-varying-order differential allows us to have more details about the curve evolution. So our segmentation result is more delicate and closer to the image boundary. And our model can segment images with intensity inhomogeneity. We can see our model is much more robust to initialization from the experimental results. From the segmentation results of noised and blurred images, we can see that our model has better performance than the CV model, the LBF model and the LIC model.

ACKNOWLEDGMENT

The authors would like to thank for the Key Projects of the Joint Fund of the National Natural Science Foundation of China under Grants No.U1833203 and the Key Research Project of the Henan Provincial Higher Education under Grants No.20A510011.

REFERENCES

[1] G. R. Senthilkumar, C., "A fuzzy clustering based mri brain image segmentation using back propagation neural networks," *Cluster Computing*, vol. 22, pp. 12 305C–12 312, 2019.

[2] Y. Shi *et al.*, "A novel clustering-based image segmentation via density peaks algorithm with mid-level feature," *Neural Computing and Applications*, vol. 28, pp. 29 – 39, 2017.

[3] X. Pan, Z. Zhang *et al.*, "Graph-based rgb-d image segmentation using color-directional-region merging," *ICASSP 2019 - 2019 IEEE International Conference on Acoustics, Speech and Signal Processing (ICASSP)*, pp. 2417–2421, 2019.

[4] J. Bragantini, S. B. Martins, C. Castelo-Fernandez, and A. X. Falcão, "Graph-based image segmentation using dynamic trees," *Progress in Pattern Recognition, Image Analysis, Computer Vision, and Applications*, pp. 470–478, 2019.

[5] P. M. Krishnammal and S. Raja, "Convolutional neural network based image classification and detection of abnormalities in mri brain images," *2019 International Conference on Communication and Signal Processing (ICCSP)*, pp. 0548–0553, 2019.

[6] A. Veeramuthu, S. Meenakshi, and K. Ashok Kumar, "A neural network based deep learning approach for efficient segmentation of brain tumor medical image data," *Journal of Intelligent and Fuzzy Systems*, vol. 36, pp. 4227–4234, 2019.

[7] L. Wang *et al.*, "Active contours driven by edge entropy fitting energy for image segmentation," *Signal Processing*, vol. 149, pp. 27–35, 2018.

[8] K. D. X. Weng, "Active contours driven by region-scalable fitting and optimized laplacian of gaussian energy for image segmentation," *Signal Processing*, vol. 134, pp. 224–233, 2017.

[9] V. Caselles, R. Kimmel, and G. Sapiro, "Geodesic active contours," *Int. J. Comput. Vis.*, vol. 22, pp. 61–79, 1997.

[10] M. Kass, A. Witkin, and D. Terzopoulos, "Snakes: active contour models," *Int. J. Comput. Vis.*, vol. 1, pp. 321–331, 1988.

[11] T. Chan and L. Vese, "Active contours without edges," *IEEE Trans. Image Process.*, vol. 10, pp. 266–277, 2001.

[12] L. Vese and T. Chan, "A multiphase level set framework for image segmentation using the mumford and shah model," *Int. J. Comput. Vis.*, vol. 50, pp. 271–293, 2002.

[13] S. W. A. Tsai, A. Yezzi, "Curve evolution implementation of the mumfordcshah functional for image segmentation, denoising, interpolation, and magnification," *IEEE Trans. Image Process.*, vol. 10, pp. 1169–1186, 2001.

[14] D. Mumford and J. Shah, "Optimal approximations by piecewise smooth functions and associated variational problems," *Commun. Pure Appl. Math.*, vol. 42, pp. 577–685, 1989.

[15] C. Li *et al.*, "Implicit active contours driven by local binary fitting energy," *Proceedings of the 2007 IEEE Conference on Computer Vision and Pattern Recognition*, pp. 1–7, 2007.

[16] K. Zhang *et al.*, "A level set approach to image segmentation with intensity inhomogeneity," *IEEE Trans.Cybern*, vol. 46, pp. 546–557, 2015.

[17] S. Liu and Y. Peng, "A local region-based chancvese model for image segmentation," *Pattern Recognition*, vol. 45, pp. 2769–2779, 2012.

[18] X. Wang, D. Huang, and H. Xu, "An efficient local chancvese model for image segmentation," *Pattern Recognition*, vol. 43, pp. 603–618, 2010.

[19] E. Cuesta and J. Codes, "Image processing by means of a linear integrodifferential equation," *Proc. 3rd IASTED Int. Conf. Visualization, Imaging, Image Process*, pp. 438–442, 2003.

[20] B. Mathieu *et al.*, "Fractional differentiation for edge detection," *Signal Process.*, vol. 83, pp. 2421–2432, 2003.

[21] Z.Ren, "Adaptive active contour model driven by fractional order fitting energy," *Signal Process.*, vol. 117, pp. 138–150, 2015.

[22] B. Chen *et al.*, "A fractional order derivative based active contour model for inhomogeneous image segmentation," *Applied Mathematical Modelling*, vol. 65, pp. 120–136, 2019.

[23] C. Li, C. Xu, C. Gui, and M. Fox, "Distance regularized level set evolution and its application to image segmentation," *IEEE Trans. Image Process.*, vol. 19, pp. 3243–3254, 2010.

[24] C. Li *et al.*, "A level set method for image segmentation in the presence of intensity inhomogeneities with application to mri," *IEEE Trans. Image Process.*, vol. 20, pp. 2007–2016, 2011.